RESULTS FROM THE PLUTO EXPERIMENT ON E^+E^- REACTIONS AT HIGH ENERGIES

Ch. Berger
1. Physikalisches Institut der RWTH
Sommerfeldstr.
5100 Aachen, Germany

Summary

Results on e^+e^- interactions at CM energies of the e^+e^- system > 10 GeV are discussed. A QED test down to very small distances ($r \approx 3 \cdot 10^{-16}$cm) was performed. The total cross section for e^+e^- annihilation into hadrons was measured. The event topologies were studied in detail. From these data we can exclude the contribution of a standard top quark. This result is supported by our measurement of inclusive muon production. Evidence for hard gluon bremsstrahlung in e^+e^- annihilation into hadrons is presented. The evidence comes from jet broadening and the production of events with 3 well separated hadronic jets.

The so called two photon reactions $e^+e^- \rightarrow e^+e^- + X$ where X is a hadronic state or a lepton pair, were measured for the first time at high invariant masses W_X. The results for lepton pair production agree very well with QED predictions. The dependence of the hadronic cross section on Q^2 (the mass of one of the virtual photons) and W_X is discussed.

Introduction

In this talk I will report on data taken with the detector PLUTO at the storage ring PETRA (Hamburg, Germany) since November 1978. The CM energy of the e^+e^--system ranges from 13 GeV up to 31.6 GeV [14,15,16].

PLUTO at PETRA is run by a collaboration of physicists from Germany, Norway and the US. The present list of authors is given below.

PLUTO Collaboration

Ch. Berger, H. Genzel, R. Grigull, W. Lackas, and F. Raupach
I. Physikalisches Institut der RWTH Aachen[1], Germany

A. Klovning, E. Lillestöl, E. Lillethun and J.A. Skard
University of Bergen[2], Norway

H. Ackermann, G. Alexander[3], F. Barreiro, J. Bürger, L. Criegee, H.C. Dehne, R. Devenish[10], A. Eskreys[4], G. Flügge, G. Franke, W. Gabriel, Ch. Gerke, G. Knies, E. Lehmann, H.D. Mertiens, K.H. Pape, H.D. Reich, B. Stella[5], T.N. Ranga Swamy[6], U. Timm, W. Wagner, P. Waloschek, G.G. Winter and W. Zimmermann
Deutsches Elektronen-Synchrotron DESY, Hamburg, Germany

O. Achterberg, V. Blobel[13], L. Boesten, H. Kapitza, B. Koppitz, W. Lührsen, R.Maschuw[12] R. van Staa and H. Spitzer
II. Institut für Experimentalphysik der Universität Hamburg[1], Germany

C.Y. Chang, R.G. Glasser, R.G. Kellogg, K.H. Lau, B. Sechi-Zorn, A. Skuja, G. Welch and G.T. Zorn[7]
University of Maryland[8], Collegepark, USA

A. Bäcker, S. Brandt, K. Derikum, A. Diekmann, C. Grupen, H.J. Meyer, B. Neumann, M. Rost and G. Zech
Gesamthochschule Siegen[1], Germany

T. Azemoon[9], H.J. Daum, H. Meyer, M. Rössler, D. Schmidt and K. Wacker[11]
Gesamthochschule Wuppertal[1], Germany

I will talk on the following topics

I	Description of the detector
II	QED results
III	Search for a new flavour threshold
IV	Investigation of gluon bremsstrahlung
V	First results on two photon interactions

I Description of the detector

The main components of PLUTO are
(A) a central detector with 13 cylindrical proportional chambers operating in a magnetic field of 1.65 T. The momentum resolution for charged tracks is $\sigma_p/p = 3\%\ p$ (p in GeV) for p > 3 GeV.

(B) barrel and endcap shower counters with proportional tubes for position measurement of the showers. The energy resolution for electrons and photons with energy E > 1 GeV is $\sigma_E/E \sim 35\%/\sqrt{E}$ (E in GeV) in the barrel and $\sim 19\%/\sqrt{E}$ in the endcaps. The geometrical acceptance of (A) and (B) is 87% and 94% of 4 π sterad.

(C) a muon identifier with a 1 m iron absorber for hadrons. The tracks are sampled at two depths within the absorber by a set of proportional and drift chambers.

(D) Forward spectrometers on each side of the detector for luminosity measurements and for selection of reactions coming from two photons interactions. Because these spectrometers are relatively new and some understanding of their operation is essential for the results of chapter V, I will describe them in more detail.

The layout of the PLUTO detector is shown in fig. 1.

Each arm of the forward spectrometers consists of a 'large angle tagger' (LAT) and a 'small angle tagger' (SAT). The LAT covers the polar angle region between 70 and 260 mrad The energy of electrons and photons is determined with a lead scintillator shower counter of 14.5 radiation length thickness. The position of charged particles is determined by six planes of proportional tube chambers with a wire spacing of 1 cm. The SAT covers the angular region between 23 and 70 mrad. Energy information of electrons and photons is obtained from a lead glass shower counter matrix. It consists of 96 blocks (each with a front area of 6.6 x 6.6 cm^2), in a concentric arrangement around the beam pipe. The thickness of this counter is 12.5 radiation length. Tracking of charged particles is achieved by a set of four planar proportional wire chambers (wire distance 0.3 cm). In a test beam the energy resolution of the LAT was measured to be $11\%/\sqrt{E}$ (rms) and of the SAT $8.5\ /\sqrt{E}$ (rms), E in GeV. These values have been reproduced by analyzing small angle Bhabha scattering.

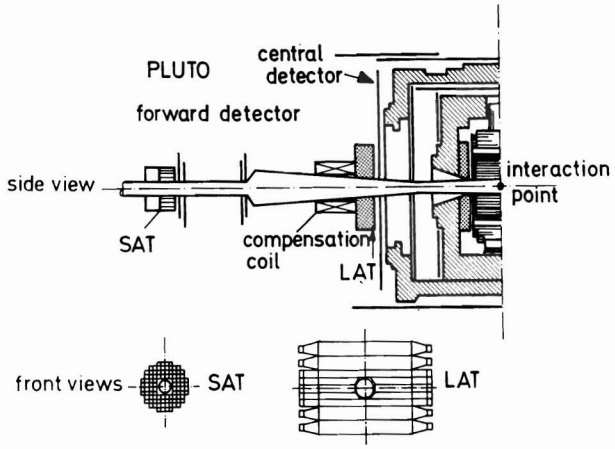

Fig.1 Layout of the PLUTO detector (only one half shown)

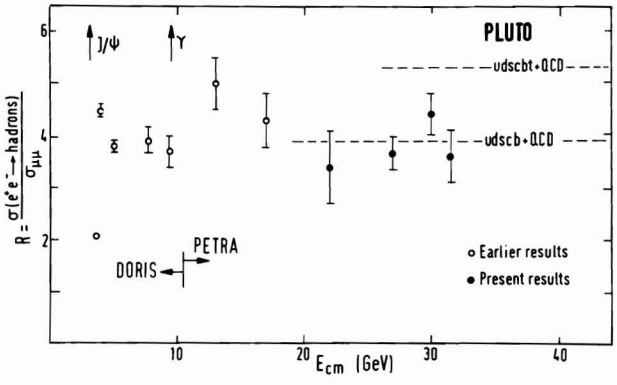

Fig.3 The ratio $\sigma^{had}/\sigma_{\mu\mu}$ versus E_{CM}. Model predictions are included.

II QED results

A high energy e^+e^- storage ring is an ideal tool for testing the validity of QED in purely electromagnetic processes at large momentum transfers.
At PETRA we have analyzed until now Bhabha scattering ($e^+e^-\to e^+e^-$) at CM energies of 13, 17 and 27.4 GeV.
In the first step of the analysis Bhabha events were defined mainly by requiring two collinear and coplanar (with the beam axis) showers in the barrel shower counter and the endcap. We required at least 1/3 of the beam energy deposited in each shower, the acollinearity and acoplanarity angle being less than 20°. For the final angular cuts we used the track information. In addition the track information served for the discrimination of very narrow hadronic jets from Bhabha scattering. Because these jets normally have a high charged multiplicity, events with more than 4 tracks originating from a common vertex were rejected. We compare our results to radiatively corrected QED predictions. The radiative corrections were computed according to Berends et al.[17], including hadronic vacuum polarisation and heavy lepton contributions.
I want to point out, that due to the strong magnetic field and good momentum resolution PLUTO can distinguish between forward and backward Bhabha scattering. For a quantitative comparision with QED we used the data between $\cos\theta = -.75$ and $\cos\theta = +.75$ (θ is the polar angle of the tracks, measured with respect to the beam axis).

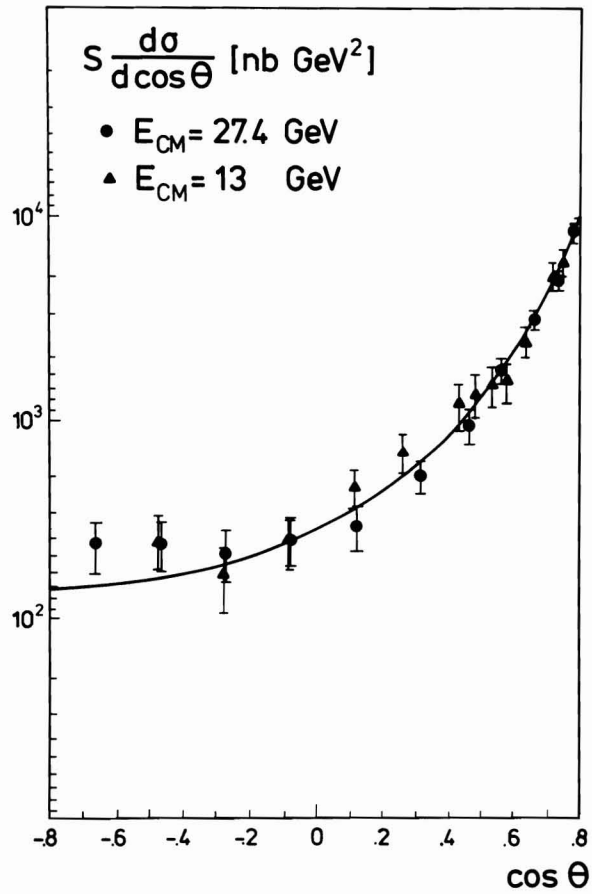

Fig.2 Angular distribution for Bhabha scattering at two energies

The energy scaled angular distributions for E_{CM} = 13 and 27.4 GeV are shown in fig.2. The agreement with QED is excellent.
For establishing quantitative limits on the validity of QED we used a form factor ansatz for the timelike (F_T) and spacelike (F_S) amplitude contributing to Bhabha scattering:

$$F_T(s) = \frac{1}{1 \mp \frac{s}{\Lambda_T^2}} \approx 1 \pm \frac{s}{\Lambda_{T\pm}^2} \quad (\text{for } \Lambda_T^2 >> s)$$

$$F_S(q^2) = \frac{1}{1 \mp \frac{q^2}{\Lambda_{S\pm}^2}} \approx 1 \pm \frac{q^2}{\Lambda_{S\pm}^2} \quad (\text{for } \Lambda_S^2 >> |q^2|)$$

(Herein $s = E_{CM}^2 = 4\, E_{beam}^2$ and $q^2 = -s \cdot \sin^2 \theta/2$)

The approximation on the right hand side gives a model independent parametrization of a possible QED breakdown.
Note, that other groups use different parametrizations [18].

Our results are summarized in table 1 for $\Lambda_S = \Lambda_T$. We have also included the DORIS data at 9.4 GeV on Bhabha scattering and on $e^+e^- \to \mu^+\mu^-$. A combined fit yields Λ_+ = 71 GeV and Λ_- = 67 GeV, thus proving QED valid down to distances of about $3 \cdot 10^{-16}$ cm.

III. Search for new flavour thresholds

In this chapter and in chapter IV I will concentrate on our data on e^+e^- annihilation into hadrons. The trigger conditions used are essentially the same as described in ref.[14]. To select hadronic e^+e^- annihilation events from our raw data we applied the following cuts

a) number of charged tracks in the central detector ≥ 2. We required a distance < 20 mm from the beam axis and < 50 mm from the interaction point, when measured along the beam (z - axis).

b) difference in azimuthal angle (ϕ) for two prongs $\Delta\phi < 150^o$

c) total observed energy (charged + neutrals) $> 0.5\ E_{CM}$. In the analysis of our 13 and 17 GeV data we actually used $E_{neutral} > 0.3\ E_{CM}$.

The observed events have a non negligible contribution from beam gas reactions (electroproduction), two photon annihilation into hadrons, and $\tau^+\tau^-$ pair production.

a) The small (<5%) background from beam gas interactions was estimated by measuring the distribution of reconstructed event vertices along the z-axis.

b) Hadron production from the so called two photon reactions i.e. $e^+e^- \to e^+e^-$ +hadrons is discussed in some detail in chapter V. We used the results obtained there for estimating the background to the annihilation channel.

c) The relative contribution from $\tau^+\tau^-$ pair production based on the prong number and neutral energy distribution was also estimated. It turned out to be rather small (<1%). In table 2 the number of observed hadronic events (corrected for beam gas background) is given for various CM energies together with the expected background from two photon reactions and $\tau^+\tau^-$ pair production.

In column 2 of the table the corresponding integrated luminosities are given. The luminosity values have been determined from Bhabha events in the central detector. They agree with the results from the forward spectrometers within 7%.

The acceptance ε of the detector (column 4 of table 1) has been calculated from a Monte Carlo simulation. I will discuss this program below. Knowing the corrections from initial state radiation, the total hadronic cross section σ^{had} can now be calculated without difficulty. As usual we compute the dimensionsless quantity $R = \sigma^{had}/\sigma_{\mu\mu}$ (column 7 of table 1). The result is plotted in fig.3 versus E_{CM}. We have also included PLUTO data at lower energies.

As indicated in the figure the R values above 22 GeV agree very well with the expected value of 3.9 obtained from udscb quarks and QCD corrections [19]. On the other hand they are clearly below the expectation including a charge 2/3 top quark. I think that a top mass of about 10 GeV (e = 2/3!) can be excluded by the R measurement alone ($\langle R \rangle = 3.88 \pm 0.22$).
The topological details of hadronic events provide an independent evidence for the presence of any new flavour threshold. This is especially important for top masses around 15 GeV, where the total cross section data suffer from the limited statistics.
We have analyzed the "jetiness" of our events in terms of the two most popular variables sphericity

$$S = 3/2 \min \sum_i p_{\perp,i}^2 \Big/ \sum_i p_i^2$$ and thrust

$$T = \max \sum_i |p_{\parallel,i}| \Big/ \sum |p_i|$$

We used both charged and neutral particles for the determination of S and T. The result for the observed S versus E_{CM} is shown in fig. 4. The data agree well with the expectation from a Monte Carlo simulation including udscb quarks (and gluon bremsstrahlung). The horizontal bars in the figure indicate the Monte Carlo values including a 'standard top quark' ($t\bar{t}$ threshold 2 GeV below E_{CM}). These expectations are definitely in conflict with the data. (~5 std.dev.) Note however, that a charge of 1/3 would reduce the difference in the expected S values by a factor 4! One arrives at the same conclusion by studying the observed thrust distribution (fig. 5). As usual we plot 1-T versus E_{CM}. The figure also includes the Monte Carlo expectations with and without the top quark.

At this stage some explanations about the Monte Carlo program are in order. The program generates events which are subsequently passed through a complete detector simulation program and the same event recognition and analysis chain as used for the data. Initial

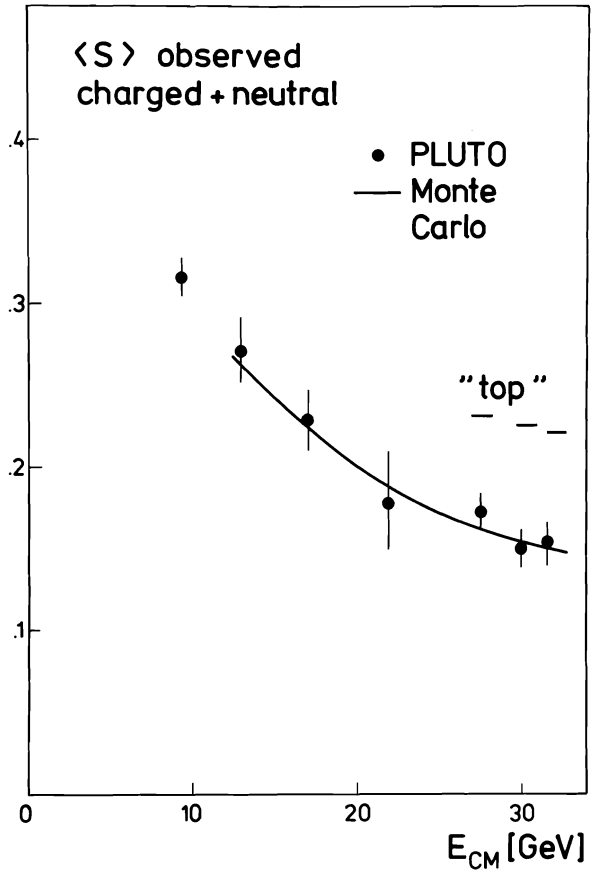

Fig.4 Observed sphericity versus E_{CM}. Model predictions with and without top quark included.

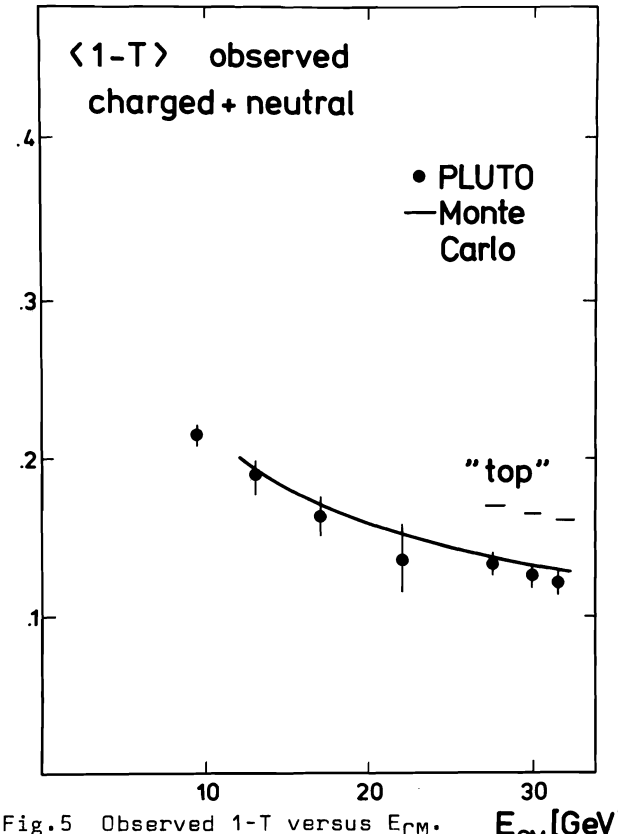

Fig.5 Observed 1-T versus E_{CM}. Model predictions with and without top quark included.

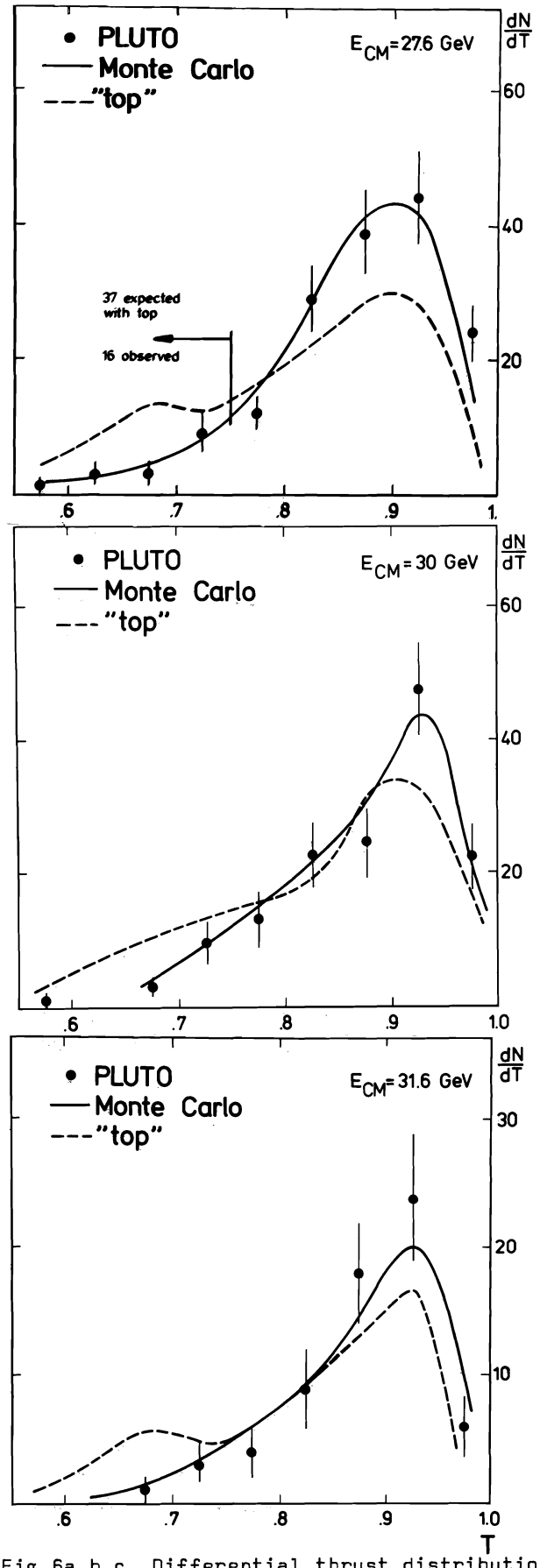

Fig.6a,b,c Differential thrust distributions at various energies. Solid line corresponds to the standard model. Dashed line includes top quarks.

TABLE 1: Limits on the QED cutoff parameters (95% confidence level)

Data used	E_{cms} (GeV)	Model	at 95% c.l. (GeV)		χ^2/DF
ee only	9.4	$\Lambda_s = \Lambda_T$	$\Lambda_+ > 43$	$\Lambda_- > 40$	19.4/23
	13		$\Lambda_+ > 29$	$\Lambda_- > 17$	10.4/14
	17		$\Lambda_+ > 55$	$\Lambda_- > 45$	8.55/13
	27.4		$\Lambda_+ > 40$	$\Lambda_- > 60$	4.26/8
μμ only	9.4		$\Lambda_{T+} > 16$	$\Lambda_{T-} > 31$	8.66/11
ee and μμ	all above energies combined	$\Lambda_s = \Lambda_T$	$\Lambda_+ > 71$	$\Lambda_- > 67$	74/64

TABLE 2: Relative hadronic cross section $R = (\sigma^{had}/\sigma_{\mu\mu})$ at specified e^+e^- c.m. energies. Background subtraction, correction for initial state radiation and τ subtraction are incorporated. The data at 13 and 17 GeV have been analyzed using slightly different methods[14] and are therefore not included in this table.

E_{CM} (GeV)	$\mathcal{L} = \int L\,dt$ (b) (nb^{-1})	N_{had} observed	ε	expected background $N(2\gamma)$	$N'(\tau^+\tau^-)$	radiative corrections δ	R (a)
22.0	47 ± 5	29	0.86	0.8	0.7	0.1	3.41 ± 0.73
27.6	408 ± 15	169	0.84	7.0	3.9	0.1	3.64 ± 0.31
30.0	561 ± 19	227	0.81	9.4	4.2	0.1	4.38 ± 0.37
31.6	219 ± 13	66	0.80	3.7	1.5	0.1	3.59 ± 0.52

(a) $$R = \frac{E_{cm}^2}{87\mathcal{L}} \left\{ \frac{(N_{had} - N_{2\gamma})}{\varepsilon} - N'_{\tau^+\tau^-} \right\} \frac{1}{(1+\delta)} ,$$

ε = detection efficiency; $N'_{\tau^+\tau^-} = \frac{N_{\tau^+\tau^-}}{\varepsilon_\tau}$

(b) Luminosity values as determined from the central shower counters. The errors are statistical. There is an additional systematic error of 5%.

TABLE 3: Comparison of inclusive muon signal with expectations from u,d,s,c,b and u,d,s,c,b,t quarks

E_{CM} (GeV)	events with a muon (p>2 GeV)	computed background	corrected signal	expected udscb	expected udscbt
27.6	7	2.9±0.8	4.1±2.7	4.7	14.6
30.0	8	4.1±1.2	3.9±3.1	5.1	15.9
31.6	2	1.7±0.5	0.3±1.5	1.7	5.3
total	17	8.7±2.6	8.3±4.9	11.5	35.8

state radiative effects are also included in the program. The $q\bar{q}$ generating program is based on the Field-Feynman model [20]. In its standard form the program contains u,d,s,c and b quarks. The top quark can be added also. For uds quarks we use the fragmentation function $f(\eta) = 1 - A + 3A\eta^2$ with $A = 0.77$; for cb (t) quarks $f(\eta)$ = constant; $\eta = 1 - z$ and $z = p_H/p_q$ where p_H and p_q are the momentum of the primary meson and the quark respectively (ref. 20,21). The transverse momentum distribution for the quarks is assumed to be $\exp(-q^2/2\sigma_q^2)$ with σ_q = 247.5 MeV. Some times we changed σ_q to higher values. This will be indicated in the text. The decay of known primary mesons with only udsc quarks are taken from the particle data tables [22]. The decays of the bottom and top mesons are from ref. 23,24.

The program is also able to simulate gluon bremsstrahlung [25] ($q\bar{q}g$ program). Following Hoyer et al.[26] gluons are radiated only by u,d,s,c quarks, gluon jets are treated as a combination of quark-antiquark pairs, the QCD cross section is taken for $q\bar{q}g$ but a cut-off on thrust is used. (This prescription yields a gluon jet in addition to the q and $\bar{q}$ jets in 15% (25%) of the generated events at 17 GeV (30 GeV) CM energy).

The need to include gluon bremsstrahlung for a quantitative description of our data will only become clear (hopefully!) at the end of chapter IV. Nevertheless I use the $q\bar{q}g$ program already now, because leaving out the gluon effects changes the conclusions about top quark contributions in no way, but only describes the sphericity and thrust distributions less accurately.

Returning now to the question of a new flavour threshold we plot in fig. 6 a,b,c the differential thrust distributions for E_{CM} = 27.6, 30 and 31.6 GeV. The data are in very good agreement with our standard model ($q\bar{q}g$, udscb quarks). In contrast, having passed the threshold for open $t\bar{t}$ production, one would expect much more events at low thrust (say $T<0.8$) and much less at high thrust. For example at E = 27.6 we would expect 37 events but observe only 16 ± 4 events.

As a final check we study the inclusive muon signal in the hadron sample. Qualitatively one would expect an increase in the number of muons per event from the cascade decay of the top quark (fig.7). In order to reduce the background from punch through hadrons we demand a minimum momentum of 2 GeV for the associated muons. The number of events with an associated muon and the expectations without and with a top quark are given in table 3. These expectations are calculated under the assumption of a cascade decay for the heavy quarks ($t \to b \to c \to d$) with a 10% branching ratio into muons at each step. The data in the energy range 27.6 to 31.6 GeV agree well with the expectations for udscb quarks and are significantly (~ 5.6 std.dev.) below the values when top quark states are included.

There are other interesting things, which one can study in our hadron sample, but which are not so closely related to the top search. As an example the averaged charged multiplicity n_{ch} (corrected for acceptance losses) is plotted versus E_{CM} in fig.8. At high energies the increase is steeper than expected from a simple extrapolation of the low energy data ($\langle n\rangle = 2 + 0.7 \ln s$ [27]) It seems to follow the trend of the pp data.

In conclusion of this chapter, the value of R, the distribution in thrust and sphericity, and the data on inclusive muons exclude open $t\bar{t}$ production due to a charge 2/3 top quark with 'standard' decay and fragmentation at CM energies below 32 GeV. The statistical limitations of the present data do not allow any conclusions regarding a charge 1/3 quark heavier than the b-quark.

IV. Investigation of gluon bremsstrahlung

Hadron production in e^+e^- collision via jets is now widely believed to be 'objective evidence for quarks'. Let us recall the basic features of a jet: The average transverse momentum of the particles in a jet (with respect to the jet axis) is limited ($\langle p_\perp\rangle \approx 300$ MeV), whereas the longitudinal momentum $\langle p_\parallel\rangle$ scales with the energy E_{CM}. In fig. 9a the mean observed $p_\perp$ and $p_\parallel$ for the charged particles is plotted versus E_{CM}. The axis is taken from the thrust calculus including information from the neutral particles. (The same convention holds true for fig. 10 and fig. 12). Although the difference in the energy behaviour of $\langle p_\perp\rangle$ and $\langle p_\parallel\rangle$ is striking, one observes also a slight increase of $\langle p_\perp\rangle$ with E_{CM}. In order to investigate this effect in more detail we study a higher moment of the $p_\perp$ distribution, namely $\langle p_\perp^2\rangle$, which is more sensitive to high $p_\perp$ effects, but still rather insensitive to experimental errors.

Jet broadening is predicted in any field theory and thus is a necessary but not sufficient condition, for the validity of QCD, which predicts an increase of $\langle p_\perp^2\rangle$ like

$$\langle p_\perp^2\rangle \sim \alpha_S(s) \cdot s$$

due to gluon bremsstrahlung ($e^+e^- \to q\bar{q}g$). The PLUTO data are shown in fig.9b. The increase in $\langle p_\perp^2\rangle$ is nicely followed by the Monte Carlo prediction including gluon bremsstrahlung (solid line), whereas the Monte Carlo without gluon bremsstrahlung predicts a much weaker increase of the observed $\langle p_\perp^2\rangle$ with the center of mass energy E_{CM}. The model predictions are also included in fig.9a and obviously $\langle p_\parallel\rangle$ and $\langle p_\perp\rangle$ are not very discriminative between $q\bar{q}$ and $q\bar{q}g$. The coupling constant $\alpha_S(s)$ (α_S/π = 6.3% at E_{CM} = 30 GeV [19]) is rather small and thus the process $e^+e^- \to q\bar{q}gg$ is strongly supressed compared to $e^+e^- \to q\bar{q}g$. One expects therefore only one of the jets to be broadened due to gluon bremsstrahlung.

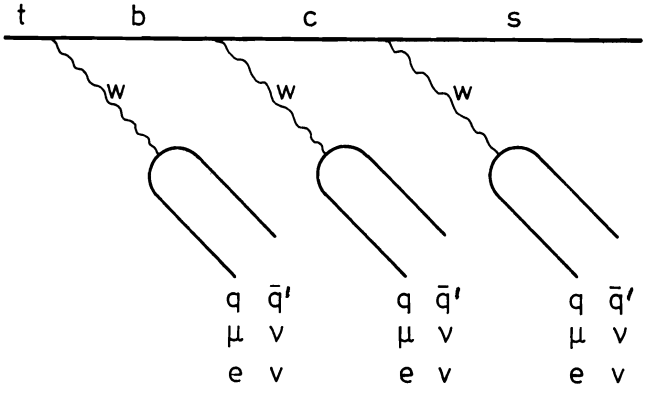

Fig.7 Cascade decay of the top quark

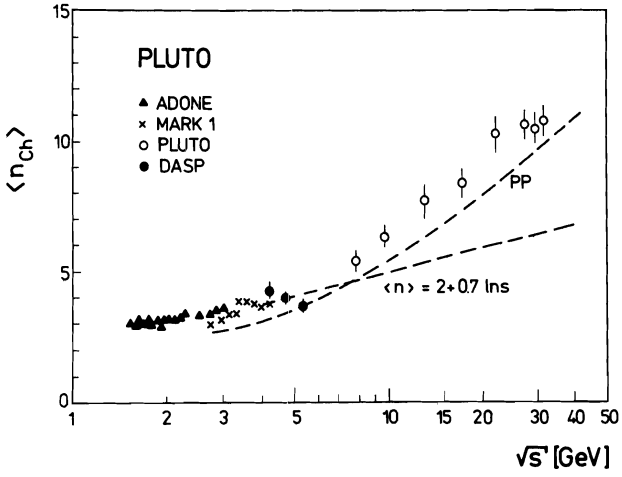

Fig.8 Average charged multiplicity versus the center of mass energy. Data from other experiments at low energies are also included.

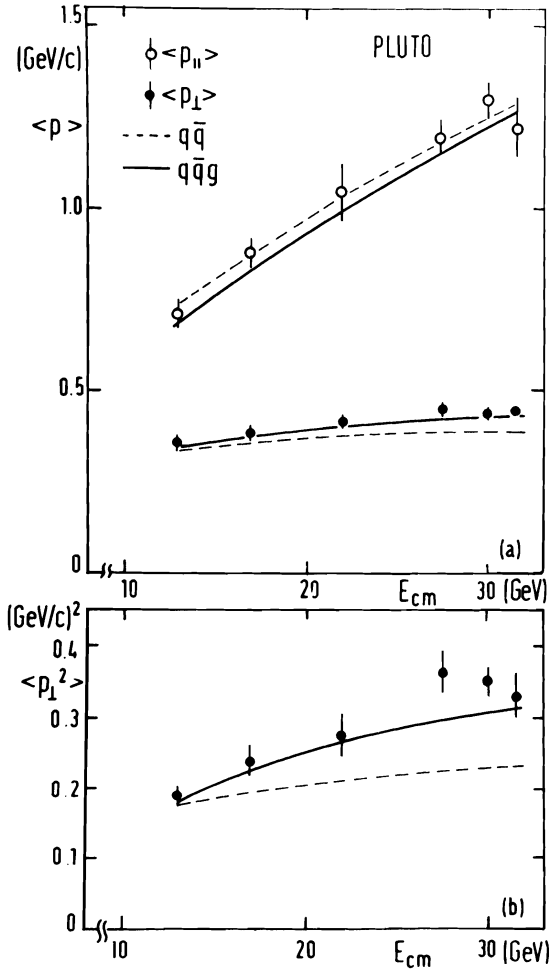

Fig.9a,b $\langle p_{\parallel} \rangle$, $\langle p_{\perp} \rangle$ and $\langle p_{\perp}^2 \rangle$ versus E_{CM} including model predictions with ($q\bar{q}g$) and without ($q\bar{q}$) gluon bremsstrahlung

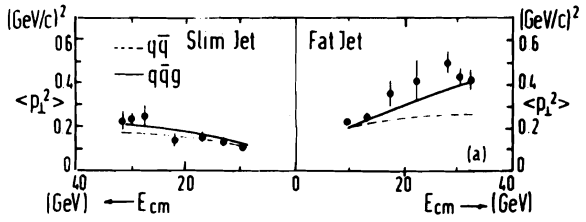

Fig.10 Average observed $\langle p_{\perp}^2 \rangle$ of charged particles in the slim and fat jet as function of CM energy.

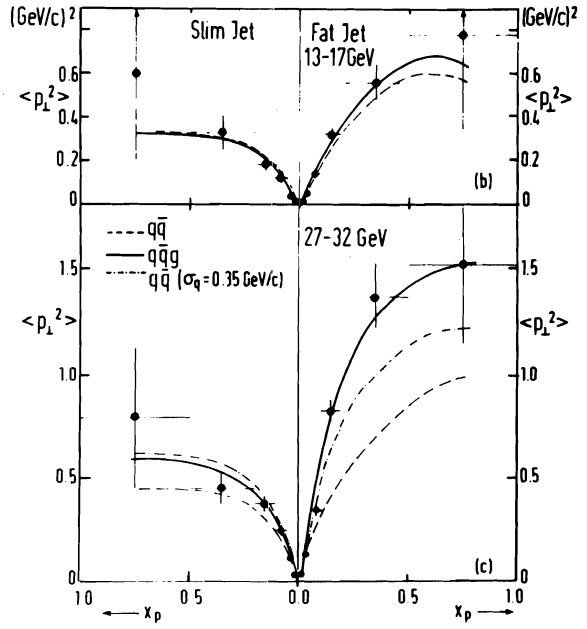

Fig.12 Seagull plots - $\langle p_{\perp}^2 \rangle$ of charged particles as function of x_p for slim and fat jets at low and high energies. The solid and dashed lines are $q\bar{q}g$ and $q\bar{q}$ predictions, respectively.

Experimentally one can search for this 'one sided jet broadening' by sorting event by event the jet with the higher $p_\perp$ into the 'fat jet' class and the jet with the lower $p_\perp$ into the 'slim jet' class. Although this procedure introduces a natural bias, the energy dependence of $\langle p_\perp^2 \rangle$ in both classes should be very different if compared to $q\bar{q}$ and $q\bar{q}g$ model predictions.

The result is shown in fig. 10. The slim jet part is equally well described by the Monte Carlo with an without gluons. On the other hand the strong increase of $\langle p_\perp^2 \rangle$ between the lowest and highest energy for the fat jet cannot at all be explained by the Monte Carlo simulation without gluon radiation.

An even more sensitive measure is obtained by investigating the dependence of $\langle p_\perp^2 \rangle$ on the scaled hadron momentum $x_p = p_h / p_{beam}$. A strong dependence of $\langle p_\perp^2 \rangle$ on x_p is again predicted from hard gluon bremmstrahlung. This follows intuitively from fig. 11.

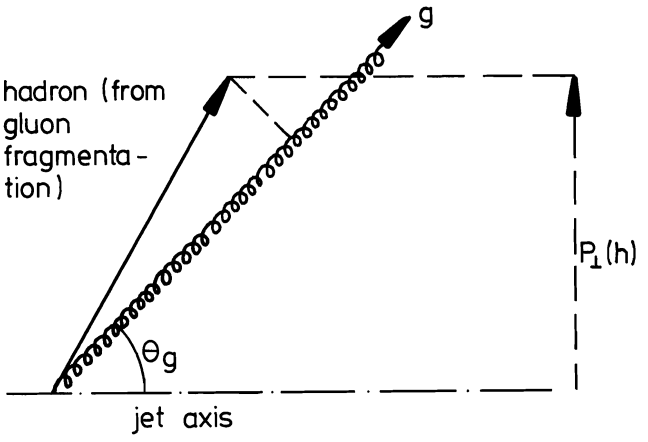

Fig.11

Because of limited statistics we combined for this research the low energy (13 and 17 GeV) and the high energy (27.6, 30, 31.6 GeV) runs. No gluon effects are visible in the so called 'seagull plot' fig. 12 for the fat and slim jet at low energies. At high energies the steep increase of $\langle p_\perp^2 \rangle$ for the fat jet can easily be explained by the $q\bar{q}g$ model, but not by $q\bar{q}$. We investigated the influence of the transverse quark momentum on our results. Trying to fit the inclusive $p_\perp$ distribution with the $q\bar{q}$ model one needs $\sigma_q \approx 350$ MeV at $E_{CM} = 30$ GeV. It is obvious from the dotted line in fig.12, that even the $q\bar{q}$ model with the artificially increased σ_q cannot fit our data.

Hard gluon bremsstrahlung should finally lead to triple jets. A nice example of a planar triple $q\bar{q}g$ jet(E_{CM}=30 GeV) is shown in fig. 13a which reminds one to the very similar

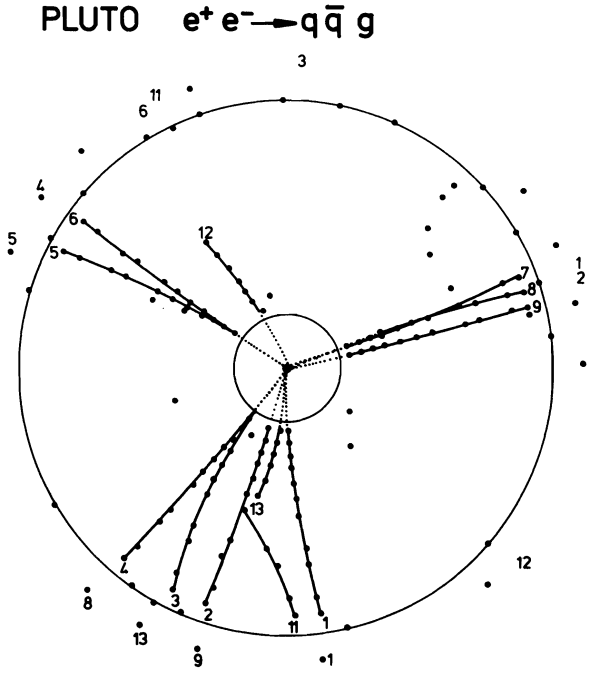

Fig. 13a

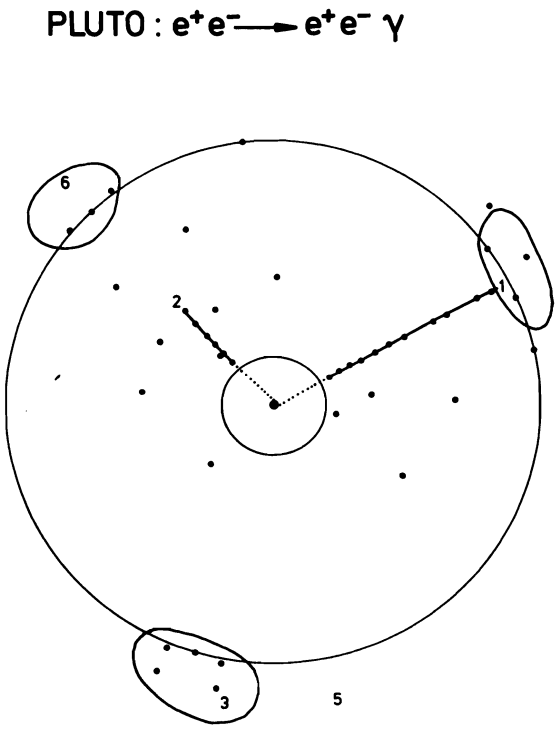

Fig. 13b

situation in radiative Bhabha scattering(eeγ), as shown in fig,13b)

For a quantitative study of the event shape we use the triplicity method [28]. The final state hadrons with the momenta $\vec{p}_1 \ldots \vec{p}_N$ (fig.14a) are grouped into 3 non empty classes C_1, C_2, C_3 with the total momenta $\vec{P}(C_1) = \sum \vec{p}_i \quad i=1,2,3, i \in C_1$

Triplicity T_3 is then defined by

$$T_3 = (1/\sum_{i=1}^{N} |p_i|) \max_{C_1,C_2,C_3} |\vec{P}(C_1)| + |\vec{P}(C_2)| + |\vec{P}(C_3)| \quad (1)$$

with the bounds $T_3=1$ for a perfect 3 jet event and $T_3=.65$ for a spherical event. Those classes C_1^* of particles yielding the maximum T_3 are identified with the hadrons originating from quark and gluon fragmentation. Thus the jet momenta are the $\vec{P}(C_1^*)$. We rename them $\vec{P}_1$, $\vec{P}_2$, $\vec{P}_3$ with $P_1 > P_2 > P_3$ ('fastest jet', second fastest jet',etc.) The convention we use for the angles between the jets is indicated in fig. 14b.

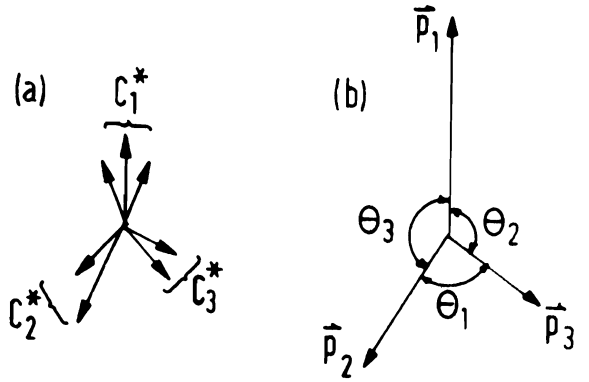

Fig.14 a,b

Triple jet events are characterized by low thrust and high triplicity. Selecting all events with $T_3>0.9$ and $T<.8$ leaves us with 48 events (for the high energy data), which has to be compared to predicted 43 events with gluon bremsstrahlung and 11 events without.
Perturbative QCD makes quantitative predictions on the cross section

$$\frac{d\sigma}{d\theta_1 d\theta_2} \quad (e^+e^- \to q\bar{q}g)$$

We investigated the jet axis orientation of our high energy data ($27.6 \leq E_{CM} \leq 31.6$ GeV) in an angular Dalitz plot. The principle is explained in fig.15. Due to the ordering procedure in fastest, second fastest and third fastest jet only the triangle ABC is filled with entries. Triple jet events are centered near C, whereas along the line AB collinear events are concentrated. A cut in θ_3 separates triple jets from $q\bar{q}$ jets. We have studied the number of entries for two different θ_3 (fig. 16) cuts and compared it to model expectations with and without gluon radiation. The results are shown in table 4. Again the agreement between experiment and the prediction based on gluon radiation is

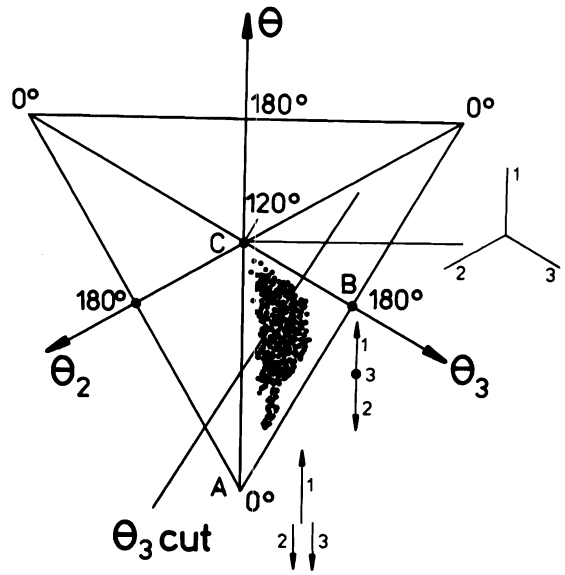

Dalitz plot for $\Theta_1, \Theta_2, \Theta_3$

$0° < \Theta_1 < 120°$
$90° < \Theta_2 < 180°$
$120° < \Theta_3 < 180°$

Fig.15 Prinziple of Dalitz plot analysis for jet axis arientation

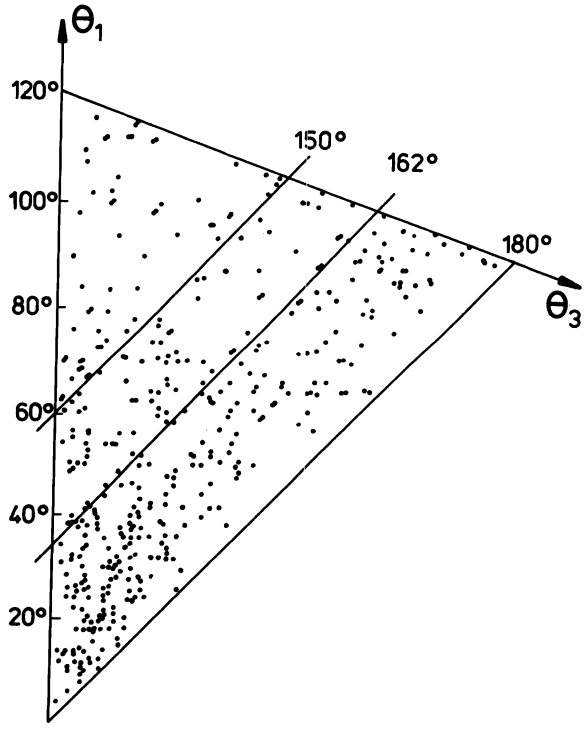

Fig.16 Event density in angular Dalitz diagram

striking, although for the rather weak cut $\theta_3<162^0$ the $q\bar{q}$ model with σ_q=350 MeV lies close to the data.

Table 4:	events observed	events expected σ_q=245MeV		events expected σ_q=350MeV
		$q\bar{q}$	$q\bar{q}g$	$q\bar{q}$
$\theta_3<150^0$	52	19	51	31
$\theta_3<162^0$	120	74	130	101

Triple jets define a plane. Therefore we expect the momentum out of the plane $\langle p^2_{out}\rangle$ to behave differently from $\langle p^2_{\perp,in}\rangle$, the transverse momentum in the plane with respect to a given axis e.g. the axis of the fastest jet. Fig. 17 shows a typical 3 jet event, demonstrating that p_{out} is rather small, but $p_{\perp,in}$ is large. (It is by the way not the same event as in fig. 13!) For a quantitative study of planarity we used the method already employed in our analysis of the τ decay [29]. We construct the conventional sphericity tensor[30]

$$T^{\alpha\beta} = \sum_{i=1}^{N} (p_i^2\,\delta^{\alpha\beta} - p_i^\alpha\, p_i^\beta) \qquad (2)$$

where the $\vec{p}_i$ are the momentum vectors of all (charged and neutral) hadrons and α,β are the coordinate indices. We now order the eigenvalues λ_k of $T^{\alpha\beta}$ so that $\lambda_1 \geq \lambda_2 \geq \lambda_3$ and call the corresponding eigenvectors $\vec{n}_1$, $\vec{n}_2$, $\vec{n}_3$. The sphericity axis is $\vec{n}_3$. If the events are disklike the normal to the disk plane is $\vec{n}_1$. The vector $\vec{n}_2$ lies in the disk plane and is normal to the sphericity axis.
We now form the averages $\langle p^2_{out}\rangle = \langle(\vec{p}\cdot\vec{n}_1)^2\rangle$ and $\langle p^2_{in}\rangle = \langle(\vec{p}\cdot\vec{n}_2)^2\rangle$ over all charged particles of an event as a measure of the momentum out of the plane and in the plane in a direction perpendicular to the sphericity axis.

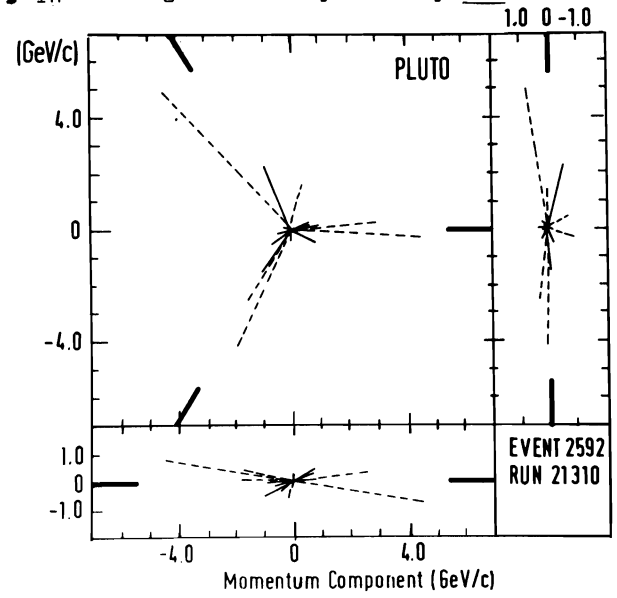

Fig.17 Momentum vectors of an event (E_{cm}=31.6 GeV) with high triplicity and low thrust projected onto the triplicity plane (top left), onto a perpendicular plane normal to the fastest jet (top right) and onto a plane containing the direction of the fastest jet (bottom). Solid and dotted lines correspond to charged and neutral particles, respectively. The directions of the jet axis are indicated as fat bars near the margins of the figures.

Fig. 18 shows the distributions of $\langle p^2_{out}\rangle$ and $\langle p^2_{in}\rangle$ for the two energy regions and for comparision the predictions of $q\bar{q}g$ and $q\bar{q}$. It is clear, that at high energies the $\langle p^2_{\perp in}\rangle$ distribution develops a tail. This tail corresponds to planar events which are predicted by $q\bar{q}g$ but cannot be accounted for by $q\bar{q}$.

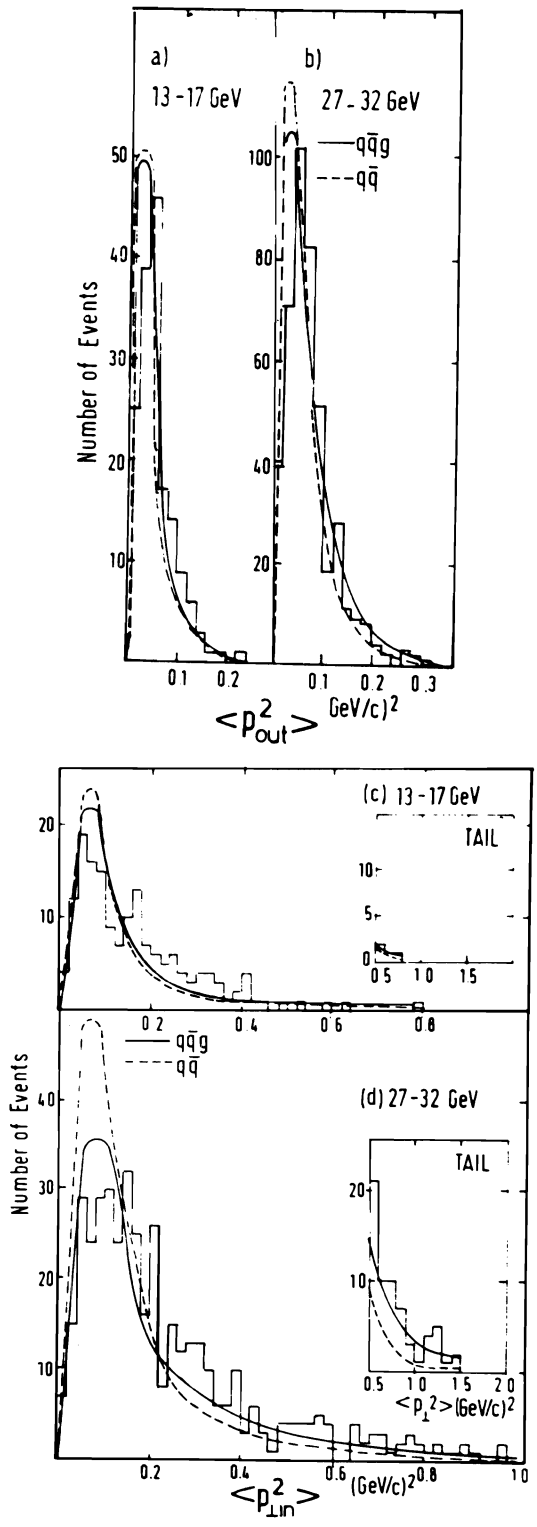

Fig.18a,b,c,d Distributions of $\langle p^2_{out}\rangle$ and $\langle p^2_{in}\rangle$ for the lower and higher energy regions. Solid and dashed lines are $q\bar{q}g$ and $q\bar{q}$ predictions respectively

We have also studied the distributions of $\langle p^2_{out} \rangle$ and $\langle p^2_{in} \rangle$ computed with respect to the normal on the triplicity plane and with respect to a unit vector in the triplicity plane perpendicular to the fastest jet axis, respectively. The results are very similar to those shown in fig.18. However, all distributions are somewhat broader, since diagonalization of (2) minimizes $p^2_{\perp}$ with respect to $\vec{n}_3$ whereas (1) maximizes $p_{\parallel}$ with respect to the 3-jet axis.

In the high energy data sample we observe 68 events with $\langle p^2_{\perp,in} \rangle > .5$ GeV^2 in good agreement with the $q\bar{q}g$ prediction of 56. In contrast the $q\bar{q}$ model (23 events) and even the $q\bar{q}$ model with σ_q=350 MeV (37 events) cannot explain the tail of the $p^2_{\perp,in}$ distribution.

To summarize this chapter, I emphasize that the evidence for gluons which has been accumulated during the past 2 years [31,32,33], especially by the work of the PLUTO group on the T resonance [29], gets very strong support from the present experiment. On the other hand we still do not have 'objective evidence for gluons'. To arrive at this goal one has (just giving one example) to be able to tell, which of the 3 jets in fig.13a is the gluon. In the case of QED (fig.13b) it is immediately obvious, which of the 3 particles is the photon. With more data to come, we will hopefully solve this problem.

V First results an two photon reactions

It was suggested some years ago[34], that in high energy e^+e^- reactions hadron production via the so called two photon mechanism (fig. 19) becomes more and more important compared to the usual 1 photon mechanism The importance of experiments covering two-photon processes lies in the fact that one can hope to extract from the measured cross section

$$e^+e^- \rightarrow e^+e^- + \text{hadrons} \qquad (3)$$

the genuine two-photon cross section for either real or virtual photons. Depending on different kinematical conditions one can explore the hadron like or the point like behaviour of photon-photon scattering in the same reaction[35]. The specific signature of reaction (3) as compared to electron-positron annihilation into hadrons is the occurence of two leptons in the final state, which are peaked at high energies and very small forward angles[36]. In order to select the $\gamma\gamma$ reactions, the PLUTO detector at PETRA has been equipped with two forward spectrometers for identifying ('tagging') the outgoing electrons and positrons (see chapter 1 for a description).

In fig.20 the distribution (beam gas-background subtracted!) of the total visible energy is shown for our data at 13.8 GeV beam energy. The cut used for separating the '1γ events' is also indicated. The steep increase towards small energies of the low energy part of the distribution strongly support the idea, that these events come from two photon reactions. This behaviour is naively expected from the bremsstrahlungs-spectrum of the interacting photons. The '2γ interpretation' becomes evident, if one looks at the energy spectrum of all events with a 'tag' (E_{tag}>3 GeV) in one of the forward spectrometers. This distribution is given by the shaded area in fig. 20.

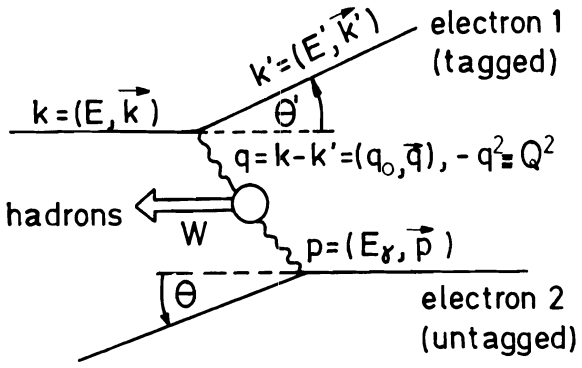

Fig.19

The vertex distribution of the tagged events (fig. 21) shows a very clear peak around the interaction point, thus excluding the possibility, that the tagged events are coming from electroproduction, with the electron scattered into the forward spectrometers.The shaded area in fig. 21 contains our candidates for hadronic events. These are defined by requiring three or more tracks in the detector or two tracks and at least one shower not associated with the tracks. The low multiplicity hadronic events have been scanned by hand, to make sure that they are not contaminated by QED background.

In order to test our quantitative understanding of two photon initiated events in the PLUTO detector, we have studied the reaction $e^+e^- \rightarrow e^+e^-$ 2 prongs. The obvious 2 prong candidates are $e^+e^-, \mu^+\mu^-, \pi^+\pi^-$.
Because the $\pi^+\pi^-$ contributions is expected to be small compared to the lepton channel, one can calculate the 2 prong cross section via high order (amplitude e^4!) QED. Fig.22 shows the distribution of the 2 prong invariant mass. The thin curve is the QED prediction using a program by Vermaseren [37]. The agreement is very good. I think the number of events in the plot and the invariant masses reached (W^2 = 16 GeV^2!) already indicate 'a big step forward' in the field of two photon physics. The analysis of the hadronic reactions was restricted to events with a tag in the SAT only, in order to keep the Q^2 of the virtual photon small.

For the question of extracting a hadronic cross section from the measured data I point out, that only the photon radiated from the untagged electron is close to the mass shell. The tagged electron, however, ($\theta' \geq 20$ mrad) radiates photons which have $Q^2 >> m_\pi^2$ ($\langle Q^2 \rangle$ up to .5 GeV^2). The proper description of this experimental situation is electron scatter-

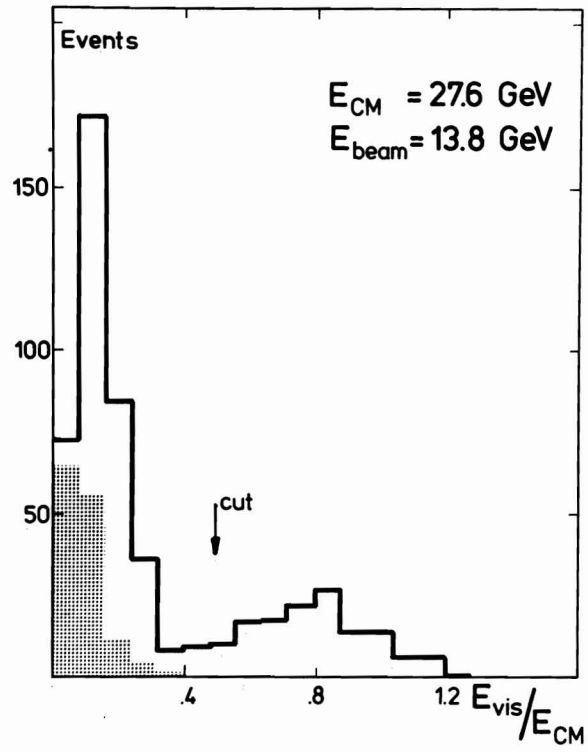

Fig.20 Distribution of the measured energy per event (charged + neutral) in units of $E_{CM} = 2\ E_{beam}$

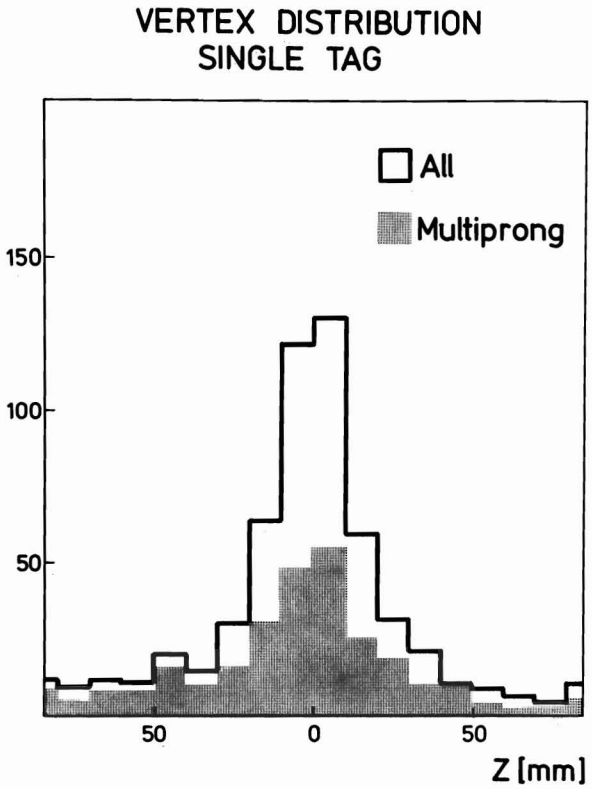

Fig.21 Distribution of event vertices for events with a tag in the forward spectrometers

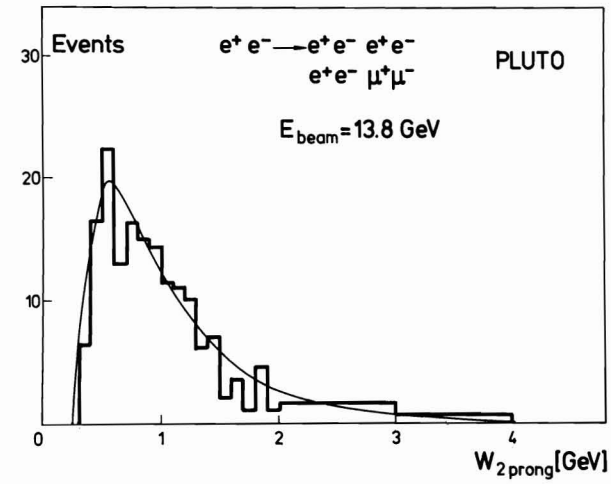

Fig.22 Distribution of the invariant mass of 2 prong events in the central detector with a tag in the forward spectrometers. The data are given by the fat histogram, the QED expectations by the thin curve.

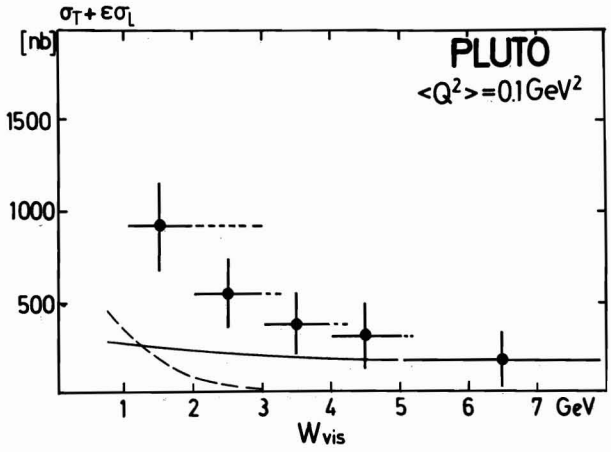

Fig.23 Total hadronic cross section for two photon initiated events at $\langle Q^2 \rangle \sim .1$GeV^2 ($E_{beam}$ = 6.5 and 8.5 GeV). Model expectations included.

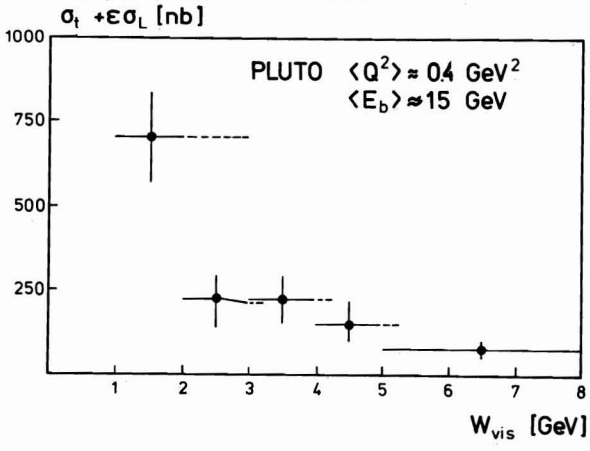

Fig.25 Total hadronic cross section for two photon initiated events at $\langle Q^2 \rangle \sim .4$GeV^2 ($13.7 < E_{beam} < 15.6$ GeV)

ing off a free photon target. The cross section for eγ scattering can be written very similar to inelastic electron-nucleon scattering. Because we want to interprete our data in terms of photon-photon cross sections rather than in terms of structure functions, we adopt, what is known as 'Hands formula' in electroproduction[38].

$$\left.\frac{d\sigma}{d\Omega'\,dE'}\right|_{e\gamma} = \Gamma_t\ \sigma_t(q^2,W^2)+\varepsilon\ \sigma_1(q^2,W^2)$$

Γ_t is aflux factor for the virtual photons, ε the polarization parameter and σ_t and σ_1 are respectively the total cross sections for hadron production via virtual transverse and longitudinal photons off a free photon target. The differential cross section for $e^+e^-\to e^+e^-$ + hadrons is then given by

$$d\sigma_{ee\to ee\ hadrons} = \Gamma_t(\sigma_t+\varepsilon\sigma_1)N(E_\gamma)dE_\gamma d\Omega'\,dE' \quad (4)$$

where $N(E_\gamma)\,dE_\gamma$ is the number of photons per electron radiated from the untagged lepton. Assuming σ_1 to be zero (which is very likely for small q^2) (4) reduces to the one term formula discussed in ref.39 but with a different flux factor. The validity of formula (4) has been discussed by Carimalo, Kessler and Parisi[40].The cross section versus W_{vis} at $\langle Q^2\rangle = .1\,GeV^2$ (E_b=6.5,8.5GeV) is shown in fig.23. W_{vis} is the invariant mass of the hadronic system as determined in the central detector, assuming pion masses for all charged particles. The range of W that contributes (FWHM) is indicated by the horizontal bars. Besides the statistical error, which is given in the figure, we estimate an overall systematic error of ±25% mainly coming from the uncertainty in the acceptance calculation. The solid line is the expectation for $\sigma_t(q^2,W^2)$ assuming a pure Regge asymptotic behaviour for γγ scattering extrapolated to low energies via duality and factorization[41]

$$\sigma_t(q^2,W^2) = (.24nb + .27nb/W)\left(\frac{1}{1+Q^2/m_\rho^2}\right)^2 \quad (5)$$

having included a ρ form factor ansatz for the virtual photon. In the highest W bins the data lie close to the model, taking into account the rather large statistical and systematic errors. This a posterori justyfies our 2γ background calculation discussed in chapter III,because the Monte-Carlo simulation used for the calculation of the 2γ contribution is based on this Regge model. In the lower bins there is an excess in the measured cross section. It is unlikely that all this excess is due to longitudinal contributions. In a recent paper[42] Greco and Shrivastava have argued that both for real and virtual photons one has to include contributions from the point-like coupling of real photons to quarks (quark-loop diagrams, fig.24). Following this suggestion and assuming an effective quark mass of 100 MeV we calculate a contribution which is given by the dotted line in fig.25. Obviously this improves the agreement with the data, but does not account for the observed cross section quantitatively.

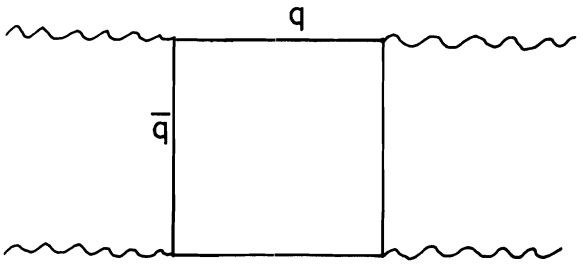

Fig.24

The hadronic cross section measured at beam energies from 13.8 to 15.6 GeV (fig.26) lie consistently below the data of fig.25. The reason is very simple. At high beam energies the average Q^2 of the electrons scattered in to the SAT is about .4 GeV^2 and thus the cross section is reduced due to form factor effects. The difference in the measured cross sections is (within the errors given) well described by the simple ρ pole ansatz of eq. (5).

To summarize this chapter, we have measured for the first time two photon initiated hadron production at center of mass energies >1 GeV. At the highest CM energies the resulting cross section is close to the expection from Regge like exchange processes, leaving room for pointlike contributions at low energies. We have also extended the measurement of two photon QED reactions to rather high invariant masses of the lepton pairs. Two photon physics will clearly be a very exciting field of research at e^+e^- machines.

Conclusions

Because I have given a summary at the end of each chapter I only emphasize the most important results again.

QED is valid down to very small distances ($\approx 3 \cdot 10^{-16}$cm)

It is very unlikely that the continuum for $t\bar{t}$ production is below 30 GeV center of mass energy.

There is evidence for gluon bremsstrahlung. Jet broadening and triple jet production rate agree with QCD predictions.

The cross section for hadron production via 2γ interactions agrees with Regge assymptotic behaviour at high CM energies. At low energies there is room for pointlike contributions.

I want to thank the organizers of the symposium for the very nice atmosphere at the conference. I have also to thank many of my PLUTO colleagues for very helpful discussions on their work.

References and footnotes

1. Supported by the BMFT, Germany
2. Partially supported by the Norwegian Research Council for Science and Humanities
3. On leave from University Tel Aviv, Israel
4. On leave from Institute of Nuclear Physics Krakow, Poland
5. On leave from University of Rome, Italy; partially supported by INFN
6. On leave from the Tata Institute, Bombay, India
7. University of Maryland General Research Board Grantee for 1978
8. Partially supported by Department of Energy, USA
9. Now at University College, London, England
10. Now at University of Oxford, England
11. Now at Harvard University, Cambridge, Mass., USA
12. Now at Technische Universität, Karlsruhe
13. Now at CERN, Geneva, Switzerland
14. PLUTO Kollaboration, Ch.Berger et.al., PL 81B (1979) 410
15. PLUTO Kollaboration, Ch. Berger et.al., DESY 79/56
16. PLUTO Kollaboration, Ch.Berger et al., DESY 79/57
17. F.A. Berends et al. NP B63 (1973) 381
    NP B68 (1974) 541
    PL 63B (1976) 432
18. L.H. O'Neill et.al.,
    PRL 34 (1975) 233
    Mark J Kollaboration, D. Barber et al.,
    PRL 42 (1979) 1110
19. We used $R_{expec} = 3 \Sigma Q_i^2 \left(1 + \frac{\alpha_S(s)}{\pi}\right)$,
    $\alpha_S(s) = 12\pi(33-2N_f)\ln(s/\Lambda^2)^{-1}$; $\Lambda = 0.5$GeV
20. R. Field and R.P. Feynman
    NP, B136 (1978) 1
21. J. Ellis, M.K. Caillard, D.V. Nanopoulos, S. Rudaz, NP B131 (1977) 285
    A. Ali, J.G. Körner, G. Kramer and J.Willrodt, DESY 79/16
22. Particle properties booklet; Particle data group April 1978
    M.K. Gaillard, B.W. Lee and J.L. Rosner
    Rev. Mod. Phys. 47 (1975) 277
    C. Quigg and J.L. Rosner
    PRD 17 (1978) 239
23. A. Ali, Z.Physik.C. Particles and Fields 1 (1979) 25 and private communication
24. A. Ali, J.G. Körner, G. Kramer and J. Willrodt, DESY 78/67 and Z.Physik C1 (1979) 203
25. J. Ellis, M.K. Gaillard and G. Ross NP B111 (1976) 253
26. P. Hoyer, P. Osland, H.G. Sander, T.F. Walsh and P.M. Zerwas, DESY 79/21, to be published
27. G. Wolf, DESY 79/71
28. S.Brandt and H.D. Dahmen Z.Phys. C1 (1979)61
29. PLUTO Collaboration, Ch. Berger et al., PL 82B (1979) 449
30. J.D. Bjorken and S.J. Brodsky, PRD1 (1970) 1416
31. C. Bromberg et al., PRL 43 (1979) 565
32. J.G.H. de Groot et al., PL 82B (1979) 292 and 456, Z. Physik C1 (1979) 143
    P.C. Bosetti et al., NP B149 (1979) 13
33. S.I. Eidelman et al., P L 82B (1979)278
34. N. Arteago Romero, A. Jaccarini and P. Kessler, C.R. Acad.Sci. B129 (1969) 153, and C.R. Acad. Sci. B269 (1969) 1129,
    V.E. Balakin, V.M. Budnev and I.F. Ginzburg, Zh. Eksp. Theor. Fiz. Pis'ma Red 11 (1970) 559 (JETP Lett. 11, 338);
    S.J. Brodsky, T. Kinoshita and H. Terazawa, PRL 25 (1970) 972.
35. E.g. S.J. Brodsky, SLAC PUB 2240 (1979)
36. If not defined in the text, the symbols used are explained in fig.1
37. We are grateful to J.A.M. Vermaseren for helping us with this program
38. L.N. Hand, PR 129 (1963) 1834,
39. S.J. Brodsky, T. Kinoshita and H. Terazawa, PRD4 (1971) 1532
40. C. Carimalo, P. Kessler and J. Parisi, College de France preprint LPC 79-17
41. E.g. S.J. Brodsky, J. Physique, C-2, Suppl.3 (1974) 69
42. M. Greco, Y.Shrivastava, N.C. 43A (1978) 88

Q and A session

Speaker: John Yoh-Columbia

Q. I have a question about one of your earlier plots on E_{vis} divided by $\sqrt{s}$. It seems to me, that if I remember properly, there is a large number of events with E_{vis} significantly less than $\sqrt{s}$. Could you show that plot again? Just how do you account for the difference between your E_{vis} and $\sqrt{s}$?

A. This plot? (Fig.20)

Q. That's right. It seems that it peaks around 0.8. Is that because you're missing a lot of events?

A. No that is due to particle losses in an event. It is a resolution effect.

Q. Oh, its resolution, I see.

Speaker: V. Lüth-SLAC

Q. Is the beam gas background subtracted?

A. Yes, in fig.20 this background is subtracted.

Speaker: J. Rosner-Minnesota

Q. What is the relation between W_{vis} and W for the two photon events?

A. It is typically about 1-2 GeV below W, but it is hard to disentangle it completely right now, We ran a Monte Carlo and found that it is typically 1-2 GeV below. (Note added: The range of W contributing to W_{vis} is now included in fig. 23 and 25)

Speaker: Arie Bodek-Rochester

Q. Can you comment on the mean multiplicity as a function of energy and how you expect it to affect the search for new specific final states?

A. We did not look for specific final states at the high energy, but I showed you the graph of the multiplicity. The multiplicity is growing rapidly, so to say. If you want, if you really want to extrapolate from the low energy regime, it seems to rise faster than lns. The charged multiplicity is now around 11 in our data at the highest possible energy.

Speaker: G. Belletini-Frascati

Q. Did you look for specific final states in the 2γ events?

A. We did a study, we looked in two prongs for example for resonances. For three and four prongs we do not find any mass peak. For two prongs we have some results.